THREE DIMENSIONAL VANE-ROTOR-VANE INTERACTION IN A ONE AND A HALF TRANSONIC TURBINE STAGE

Berardo Paradiso[1,2], *Giacomo Persico*[1], *Paolo Gaetani*[1], *O. Schennach*[2], *R. Pecnik*[2], *and J. Woisetschläger*[2].

[1] Laboratorio di Fluidodinamica delle Macchine, Dipartimento di Energia
Politecnico di Milano. Italy
berardo.paradiso@polimi.it
[2] Institute for Thermal Turbomachinery and Machine Dynamics
Graz University of Technology, Austria
jakob.woisetschlaeger@tugraz.at
http://www.ttm.tugraz.at

ABSTRACT

The current paper presents the final results of an extensive experimental and numerical clocking investigation performed in a high-pressure transonic turbine with a downstream vane row (1.5 stage machine). A transient 3D-Navier Stokes calculation was performed for two clocking positions and the three dimensional results are compared with Laser-Doppler-Velocimetry and high response pressure probe measurements at three different planes (rotor exit, second stator inlet and second stator outlet). Two selected clocking positions are discussed in detail with the focus on the interaction between the structures coming from the first stage and the second vane. Close to the leading edge of the second vane the rotor hub passage vortex enters the second stator in different circumferential position, and induces different secondary structures at the second vane exit. It results in differences in the second vane performance due to the different clocking positions.

NOMENCLATURE

A		1^{st} vane upstream
C1		rotor outlet
C2		second vane inlet
Cps=(Ps–Pref)/(Ptm–Pref)		static pressure coefficient
Cpt=(Pt–Pref)/(Ptm–Pref)		total pressure coefficient
D1		second vane outlet
Pref	[bar]	downstream reference pressure
Ps	[bar]	absolute static pressure
Pt	[bar]	absolute total pressure
Ptm	[bar]	inlet total pressure
$y=\left(\overline{\overline{Pt_{C2}}}-\overline{Pt_{D1}}\right)/\left(\overline{\overline{Pt_{C2}}}-\overline{Ps_{D1}}\right)$		2^{nd} stator loss coefficient
u	[m/s]	tip pheriferal velocity
Δh	[m^2/s^2]	static entalpy drop
Greek		
α	[deg]	blade to blade absolute flow angle (positive in peripheral direction)
δ	[deg]	rotor deviation angle

Abbreviation

CP	clocking position
Cyl	cylindrical single hole fast-response
FHP	five hole probe
LE	leading edge
LDV	laser doppler velocimetry
PS	pressure side
RBPP	rotor blade passing period
RHPV	rotor hub passage vortex
SS	suction side
TE	trailing edge
TLV	tip leakage vortex

Superscripts

=	pitchwise and spanwise average
–	spanwise average

Subscripts

R	rotor – relative

INTRODUCTION

In the last decades the study of the unsteadiness has represented one of the most important topics in the reference literature for turbomachinery. It is well known that the flow unsteadiness in turbomachinery is highly related to the vane-rotor relative motion and the wake-wake interaction. Additionally in high-pressure turbines the secondary flows, strong potential fields and trailing edge shocks must be taken into account. In this scenario Clocking represents an attempt to increase the efficiency by varying the circumferential and/or the axial position of adjacent vanes or blades. In case of one and an half stage test facilities, the most common method is to rotate the nozzle ring with respect to a reference vane row; the largest efficiency variation is obtained with equal blade counts.

In LP turbines the clocking is directly linked to the wakes (Huber et al., 1996), while in transonic HP turbines the trailing edge shocks and the secondary flows of the first vane represent a further cause of circumferential non uniformity for the downstream vane; wakes have little effects compared to other flow structures (Miller et al., 2003).

The influence of the first vane shock on the rotor aerodynamics has been investigated by a number of authors, Dénos et al. (2001) observed significant rotor load fluctuation as a consequence of the shock-rotor interaction; Gadea et al. (2004) showed, in a 1.5 HP turbine, how the optimum clocking position for aerodynamics did not minimize the unsteady force. However, Haldeman et al. (2005) observed in a HP turbine a decrease in envelope size of the static pressure for the optimum aerodynamic clocking position. Recently Paradiso et al. (2008) observed that at the first stage exit the rotor hub passage vortex as well as the rotor trailing edge shock are strongly influenced by the first vane shock.

The secondary flow interaction represents an important unsteady effect, mainly in low aspect ratio turbine stages. Sharma et al. (1992), observed a dramatic influence of the very strong rotor vortices on the second stator aerodynamics, resulting in a completely altered second stator secondary field. Recently the clocking effects driven by the first stator secondary vortices has been studied in detail in a multistage subsonic turbine (Behr et al., 2007).

The goal of the present paper is to study the interaction of the three dimensional structures coming from the first stage with the downstream vane, using both experimental and numerical tools.

TEST FACILITY

The transonic test rig operating at the Institute for Thermal Turbomachinery and Machine Dynamics at Graz University of Technology is a continuously operating cold-flow open-circuit facility and it allows to test turbine stages in full-flow similarity (corrected speed and pressure ratio). The turbine is driven by pressurized air delivered by a 3 MW compressor station; a brake compressor delivers additional air mixed to the flow from the compressor station and increases the

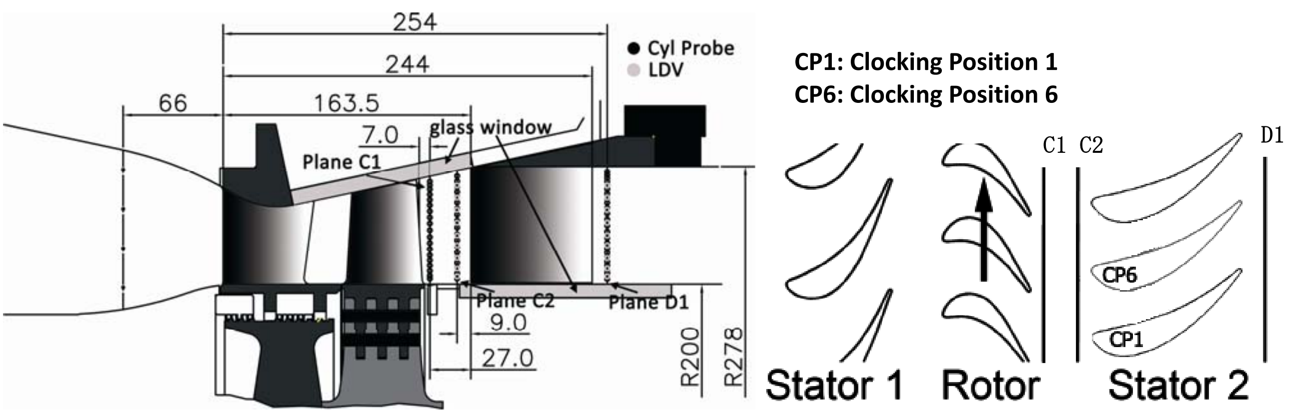

Figure 1: Meridional section with radial measurement locations (left) and investigated clocking positions (right).

overall mass flow. The air temperature in the mixing chamber (turbine stage inlet) can be adjusted by coolers between 40 °C to 185 °C. The maximum shaft speed of the test rig is limited to 11550 rpm. Depending on the stage characteristics a maximum coupling power of 2.8 MW at a total mass flow of 22 kg/s can be reached. Detailed information on the design, construction and operation of the facility can be found in Erhard and Gehrer (2000), on the operation in Neumayer et al. (2001).

Turbine Stage tested

The meridional section of the turbine stage is given in Figure 1. To provide access for all types of optical measurement techniques, contour shapes were properly chosen along the whole meridional section; the access is made by two glass windows upstream and downstream of the second vane row. To change the relative pitchwise position between the two vane rows (required for clocking analysis) and to allow optical measurements in the flow channel of the first vane close to the trailing edge, the vane has a gap of 0,8 mm at the tip in the rear part. The second vane rotation requires a radial clearance of 1 mm at the hub of the second vane. The rotor blade tip gap is also 1 mm.

Time-resolved flow velocity measurements were performed by means of Laser-Doppler-Velocimetry (LDV) in planes C2 and D1 (Figure 1). In planes C1 and C2, phase-resolved pressure measurements were performed by means of a cylindrical high response aerodynamic pressure probe (Cyl). Additionally time-averaged pneumatic measurements were performed by means of a conventional Five Hole Probe (FHP) in planes C1, C2 and D1. The different circumferential positions on the measurement traverses were achieved by rotating both stators, while the probes and the LDV-head remained at a fixed circumferential position.

Some information on the operating conditions and on the geometrical data of the stage are given in Table 1.

number of nozzle guide vanes	24	rotor tip clearance / span [%]	1.4
number of rotor blades	36	2^{nd} vane clearance / span [%]	1.3
number of 2^{nd} guide vanes	24	1^{st} vane-blade spacing [% nozzle axial chord (midspan)]	47
nozzle chord (midspan) [mm]	78.9	blade-2^{nd} vane spacing [% blade axial chord (midspan)]	73
nozzle axial chord (midspan) [mm]	56.1	stage pressure ratio	3.30
geometric turning angle nozzle [deg]	70	overall pressure ratio	4.27
nozzle aspect ratio (exit height / chord)	0.70	rotational speed [rpm]	10600
blade chord (midspan) [mm]	55.9	inlet total temperature [K]	413
blade axial chord (midspan) [mm]	46.8	Reynolds number nozzle guide vane exit	$2.57\ 10^6$
geometric turning angle blade [deg]	107	Reynolds number rotor blade exit	$1.69\ 10^6$
blade aspect ratio (exit height / chord)	1.24	isentropic 1^{st} vane exit Mach number	1.13
2^{nd} vane chord (midspan) [mm]	88.3	blade outlet Mach number, midspan	0.51
2^{nd} vane axial chord (midspan) [mm]	80.1	relative blade outlet Mach number, midspan	0.87
geometric turning angle 2^{nd} vane [deg]	53	2^{nd} vane outlet Mach number	0.69
2^{nd} vane aspect ratio (exit height / chord)	0.88	loading factor ($\Delta h/u^2$)	1.51

Table 1: Stage geometrical data and operating conditions

Laser-Doppler-Velocimetry

Flow velocity measurements were performed by a two-component LDV-system. A detailed description of the optical setup is given in Schennach et al. (2007), where a maximum error in velocity is shown to varying between 0.5% in the free-stream and 5% in the wakes. Each measurement grid consists of 20 measurement positions in circumferential direction and 9 positions in radial direction.

Cylindrical high response pressure probe

Unsteady flow measurements were performed by means of a cylindrical single-hole fast-response aerodynamic pressure probe (Cyl), operated as a virtual three sensor probe for 2D aerodynamic measurements. The measurement grid consists of 18 (C1) or 17 (C2) positions along the blade span and of 20 positions over the stator pitch.

The probe aerodynamic accuracy was evaluated in a calibrated nozzle, resulting in an extended uncertainty equal to ±0.5% of the kinetic head for the pressure measurements and equal to ±0.3 deg for the flow angle. Specific tests showed that the pressure reading of the probe is insensitive for radial flow angles inside ±10 deg. The transfer function of the line-cavity system connecting the probe tap to the pressure sensor was determined by means of tests in a low-pressure shock tube (Persico et al., 2005). The probe bandwidth is up to 80 kHz, after digital compensation. In the test rig application the instantaneous pressure signal is acquired at 1 MHz for one second, to achieve good statistical reliability. The raw pressure data are phase-locked and then phase-averaged over about 6250 periods to obtain 20 intervals on a single RBPP, corresponding to a physical sample rate of about 125 kHz (thus the physical measurement data arise from local averages of groups of eight acquired values). The flow quantities are derived from the combination of the different phase-averaged pressures through the aerodynamic calibration. The relative quantities are then calculated making use of the time-averaged total temperature. The Rankine vortex model is applied to identify streamwise vortices on the basis of only the blade-to-blade flow angle.

UNSTEADY THREE-DIMENSIONAL NAVIER-STOKES SIMULATION

The computations were performed using the Navier-Stokes code LINARS, developed at Graz University of Technology (Pecnik et al. 2004, Pecnik et al. 2006). The compressible Favre-averaged Navier-Stokes equations are solved in conservative form by means of a fully-implicit time-marching finite-volume method on structured curvilinear grids in multiblock alignment. The inviscid fluxes are discretized by the upwind flux-difference splitting method of Roe, applying a TVD scheme to achieve a high order of spatial accuracy. The viscid flux vector is constructed with a second-order accurate central-differencing scheme.

To cope with unequal pitch ratios, the code uses phase-lagged boundary conditions at geometrical periodic boundaries, and hence only one passage each blade row was simulated with a total of about 2 million cells. In this work one blade passing period was calculated with 480 time steps for the rotor and 320 time steps for both stator passages. To save computational time and memory, pressure gradient wall-functions were used for the near wall treatment. The turbulence was calculated using the one equation turbulence model of Spalart and Allmaras. Details on the numerical set-up are given in Schennach et al. (2007). It has to be reminded that the CFD mesh models the rotor tip gap but not the second vane hub leakage.

FIRST STAGE UNSTEADY AERODYNAMICS

A comprehensive discussion on the second stator aerodynamics can only be built on a detailed knowledge of the unsteady flow released by the first stage. In this section the flow in the first stage is briefly recalled; a description of the second vane inlet flow field is provided and the mechanisms promoting the clocking between the two stators are discussed. The interested reader is referred to Paradiso et al. (2008), for a detailed discussion on this topic.

Rotor inlet flow field

It is commonly found that in transonic turbines the flow downstream of the first stator is characterized by a relatively strong shock, which departs from the suction side of the trailing edge. LDV measurements and numerical simulations confirm that a strong shock also occurs in the present turbine, and plays a major role due to the high Mach number at the vane exit (~ 1.2). The viscous effects, instead, play a minor role in this case. In the LDV measurement plane just upstream of the rotor leading edge the wake appears almost mixed out due to the relatively large vane-rotor axial gap (about half of the 1st vane axial chord). Conversely the secondary flows, that are normally characterized by a much lower decay rate, do not appear in the measurement plane as very weak vortices are generated inside the channel. This feature, confirmed by the numerical simulation, is due to the dramatic acceleration experienced by the flow in the first vane (Perdichizzi, 1990) and by the aft-loaded vane profile (Weiss and Fottner, 1995). The only vortical structure visible at the first vane exit is a small core of clockwise vorticity confined at the hub endwall, which is generated by a shock-induced separation at the corner between the blade suction side and the hub endwall. At the tip, instead, no traces of vortical structures are observed in the experiments.

As a consequence, the distribution of the relative quantities at the rotor inlet is dominated by the first vane shock. In particular, the relative total pressure shows a sharp variation of pressure ratio across the shock (~ 1.25) within an almost uniform field. Moreover, since both the absolute flow angle and the velocity magnitude are modified by the shock (the two contributions constructively interfering), the relative flow angle experiences a 20 deg variation across the shock.

Unsteady rotor exit flow field

As a consequence of the large pitchwise gradients induced by the first vane shock, a significant unsteadiness affects the flow entering the rotor. The rotor aerodynamic downstream of the rotor is now discussed in the absolute frame.

In Figure 2 the instantaneous static pressure, relative total pressure and deviation angle fields are reported for two instants of the rotor blade passing period in a measurement plane close to the rotor trailing edge. In the frames, covering an annular range of two vane pitches or three rotor pitches (i.e., the actual spatial periodicity of the blade rows), the trace of the three rotor wakes are identified as radial low Cpt_R regions. The tangential static pressure gradient visible at midspan is the trace of a weak shock generated at the suction side of the rotor blade, as confirmed by CFD. The unsteadiness of the shock, which is seen to evolve from a hub-to-tip front of Cps gradient to a negligible perturbation, is caused by the periodic variation of the expansion ratio across the rotor as a consequence of the 1st vane shock sweeping (see Paradiso et al., 2008, for a discussion of the physical mechanism). However, the rotor shock strength remains generally weak and it is going to have only little influence on the downstream vane.

The wakes are enlarged at the endwalls by two low Cpt_R cores, directly connected to vortex cores (identified as strong radial gradients of relative flow angle). In particular the wide loss core at the tip is connected to the TLV, while the loss core just below midspan is connected to the RHPV. It is to be noted that, while the tip vortex is almost constant for different channels at different instants (i.e., it is almost steady in the relative frame), the loss core and the vorticity below midspan experience a significant evolution during the period, as extensively discussed in Paradiso et al.,

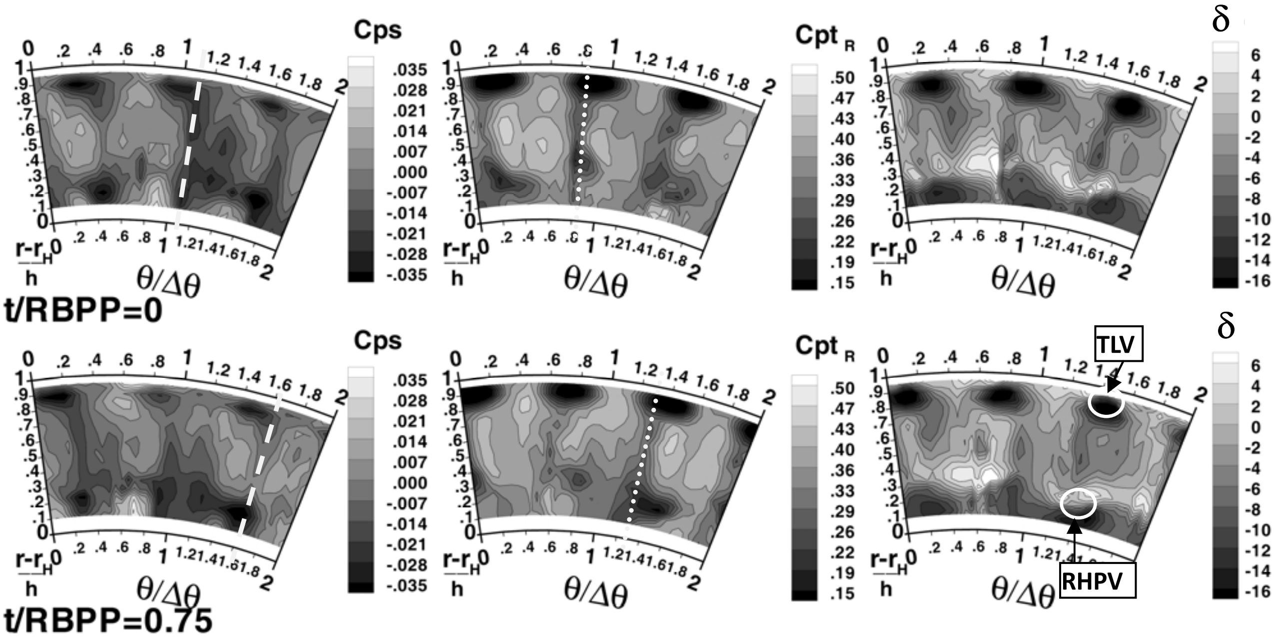

Figure 2: Cyl phase-resolved flow field downstream of the rotor in plane C1 – absolute frame.

2008. This vortex unsteadiness is characterized by high amplitude of fluctuation and low decay rate, and therefore it is going to influence the second stator aerodynamics. The 1st vane shock is thus promoting the most relevant clocking effect in this turbine.

SECOND STATOR INLET FLOW FIELD

In this section the interaction between the incoming structures with the second vane is introduced showing the time-mean pitchwise averaged result of α for two different clocking positions: CP1 and CP6. FHP and LDV results are compared all over the span with CFD.

In the following section the unsteady results of Cyl and CFD will be presented giving particular emphasis to the evolution in the hub region, where the most interesting features has been observed downstream of the first stage.

Pitchwise averaged results

In Figure 3 the α angle in plane C2 is reported. LDV and FHP show a good agreement while some differences are observed from CFD data. The tip region is influenced by the rotor tip clearance that makes the flux entering the second vane more axially. In the upper midspan region the angle does not show strong variations, only CFD at 70% span shows a local region of low α angle due to a different averaging of the secondary structures coming from the first stage. In the midspan-hub region the flow field is characterized, for both experimental and numerical approach, by an increase of the overturning. In plane C2 the time-averaged results show no significant effects induced by clocking. The agreement between experimental and numerical results in a maximum difference of about 8 deg. at 20% span.

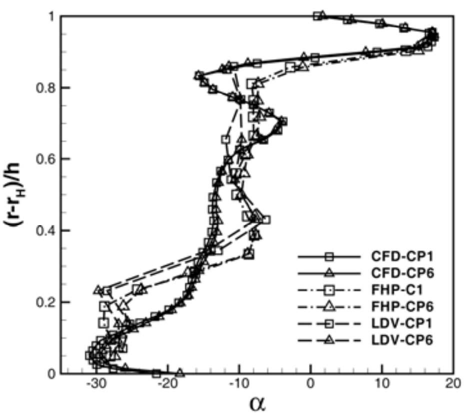

Figure 3: pitchwise averaged α angle plane C2, FHP, LDV and CFD.

Instantaneous results

In order to discuss the three-dimensional character of clocking and the coupling between the rotor structures and the second stator aerodynamic for two different clocking positions (CP1 and CP6) unsteady results from Cyl measurements and CFD are discussed. As the potential field of the vane propagates upstream, the increase of Cps over the span (not reported for sake of brevity)

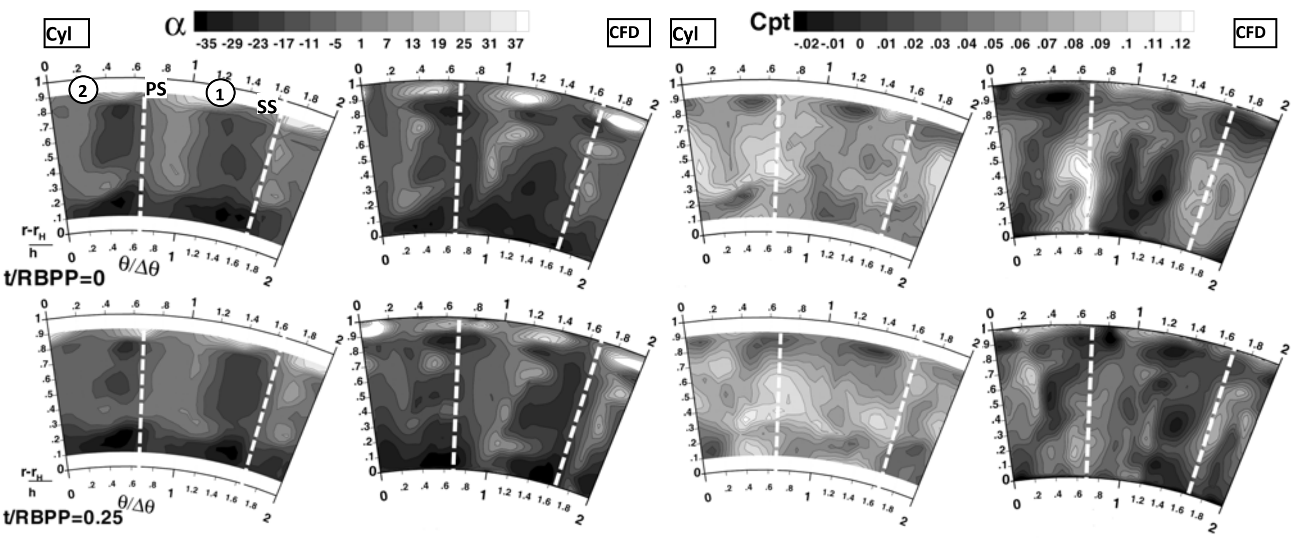

Figure 4: Instantaneous flow field in plane C2 for CP1. α angle (left), Cpt (right) for Cyl and CFD.

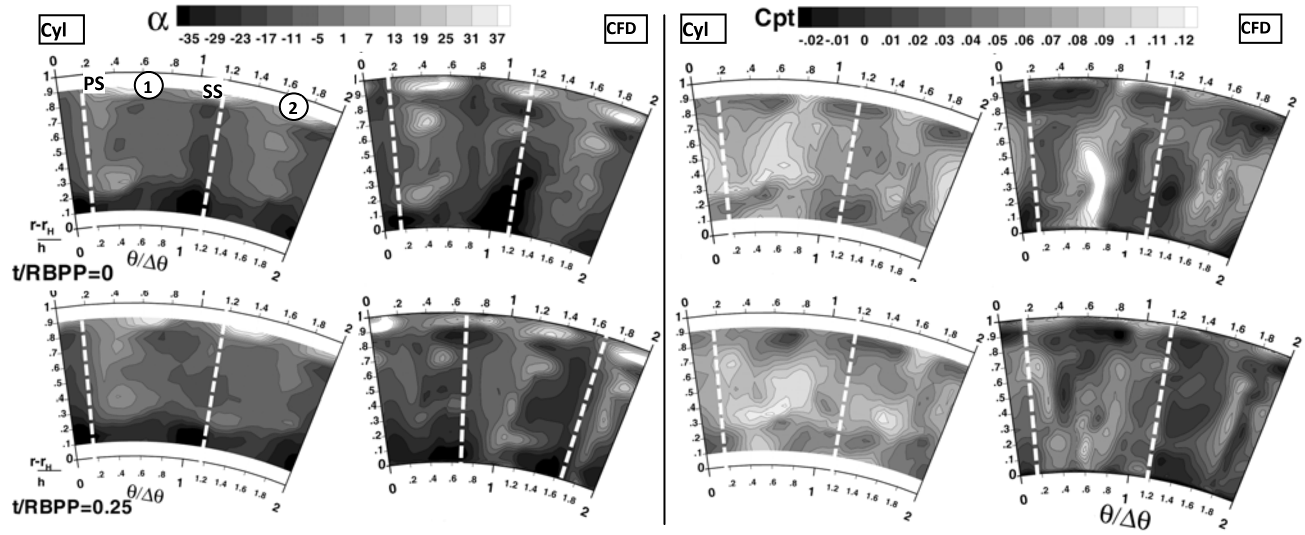

Figure 5: Instantaneous flow field in plane C2 for CP6. α angle (left), Cpt (right) for Cyl and CFD.

represents a marker of the downstream vane position, marked in Figure 4 and 5 by white dashed lines. Two different instants (t/RBPP=0 and t/RBPP=0.25) are reported in the following: due to the time-space periodicity the evolution in time of the flow field allows to have a complete representation of the rotor blade period only presenting these two instants. For this reason if we pay attention to the channel identified with the number 1 in Figure 4, the same channel experiences in the second half of the period the same evolution of the adjacent channel (2 in Figure 4) in the first half of the period.

Focusing on CP1 and looking first at Cpt (Figure 4), the tip region is dominated by a rotor periodicity (3 peaks on 2 stator passages); related to the same peak regions, high α gradients are found related to the rotor TLV, as already discussed in C1. Differently from C1 where the regions of low Cpt_R were very similar in terms of dimension and magnitude, in C2 the minima are different being affected by the second stator potential field.

Focusing on the midspan-hub region, Cpt and α show a strong modulation of the rotor hub passage vortex, identified in plane C1 on the basis of the deviation angle map, due to its periodic generation mechanism and due to the interaction with the second vane. In particular, concerning the periodic evolution of the RHPV core, marked by the regions of high α and Cpt gradients, it interacts with the second vane field impinging on the SS of the LE when it is stronger (t/RBPP=0 channel 2 θ/Δθ=0.4, 20% span); on the contrary it enters the vane at midpitch when it has low magnitude (t/RBPP=0, channel 2, θ/Δθ =1.4, 20% span) The CFD and the Cyl data presents good agreement from a qualitative as well as quantitative point of view; the location of the vortex core is well modeled by the code, corresponding to high α gradients and low Cpt peaks.

Changing the clocking position from CP1 to CP6 (see Figure 5), the tip region presents the same pattern previously commented, the weak differences being only caused by the shifted position of the second vane. Below midspan the vortex dynamics described for CP1 is still recognized at CP6 with a different effect on the second vane aerodynamic: the RHPV impinges mainly on the PS of the LE when it is stronger (t/RBPP=0, channel 2, θ/Δθ = 0.2, 20% span).

Due to the strong unsteadiness of the RHPV induced by the first vane shock, the hub region, represents a potential for improving the performance of the second vane through airfoil indexing: on the other hand the region above midspan and in particular the tip region is expected to influence only marginally the performance due to clocking.

SECOND STATOR OUTLET FLOW FIELD

This section is devoted to the presentation and discussion of the data acquired by means of FHP and LDV in plane D1 and its comparison with the numerical simulation; the discussion is introduced by an analysis of the pitchwise-averaged flow angle for two different clocking positions; then, phase–resolved LDV data and unsteady CFD results are presented to investigate the two clocking positions.

It should be reminded that the vane hub clearance of 1 mm was not modelled in the simulation.

Pitchwise averaged results

In Figure 6 the α angle in plane D1 is reported. Although CFD and FHP in this case show more pronounced differences all over the span, some common aspect could be evidenced.

The tip region is dominated by the TPV, whose time-averaged intensity is modulated among the different clocking positions by the interaction with the rotor TLV entering the channel and by the blade loading; CFD and FHP present a similar pattern with a shift of about 5 deg. Moving towards the hub, the two approaches - especially the CFD - show for the two clocking positions a significant variations of blade-to-blade flow angle, which reflects the complex secondary field downstream of the cascade.

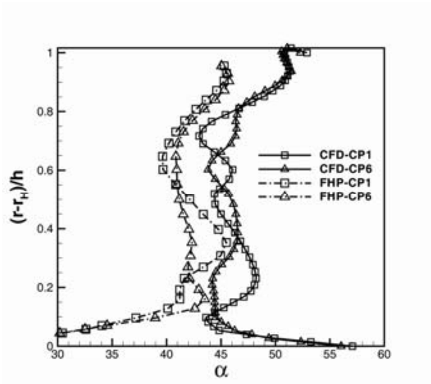

Figure 6: plane D1 pitchwise averaged α angle.

Close to the hub the presence of the gap enhances the differences between the experimental results and the CFD; in experiments strong α gradient is found in this region due to the rolling up of the hub leakage flow. It is clear that this latter feature, in the region where most potential for clocking is expected, will affect only the experimental data; on the contrary the CFD could provide a more realistic difference between the two clocking positions.

Instantaneous results

To analyse in detail the phase-resolved flow field the same instants of time discussed in plane C2 are presented in the follow for CP1 and CP6. CP1 shows a highly unsteady behaviour on all the measured quantities: the velocity field is modulated in magnitude and direction as well as periodic fluctuations of the flow angle occur in the vortex cores (Figure 7). Results from LDV compared with CFD data show different pattern at the hub due to the leakage. At t/RBPP=0 in the second channel (0.8 <θ/Δθ< 1.8), the high flow velocity in the free-stream all along the span is coupled to a region of intense α gradients at θ/Δθ=1.6 and 45% span for the LDV and 35% for the CFD (dotted circle in Figure 7). The different spanwise position of the vortex core may be caused the strong hub leakage that moves the region of low energy in radial outward direction. This vortex presents an highly unsteady behaviour weakening to almost disappear in the final part of the rotor period. Focusing now on CP6 (Figure 8) an almost steady flow field is observed

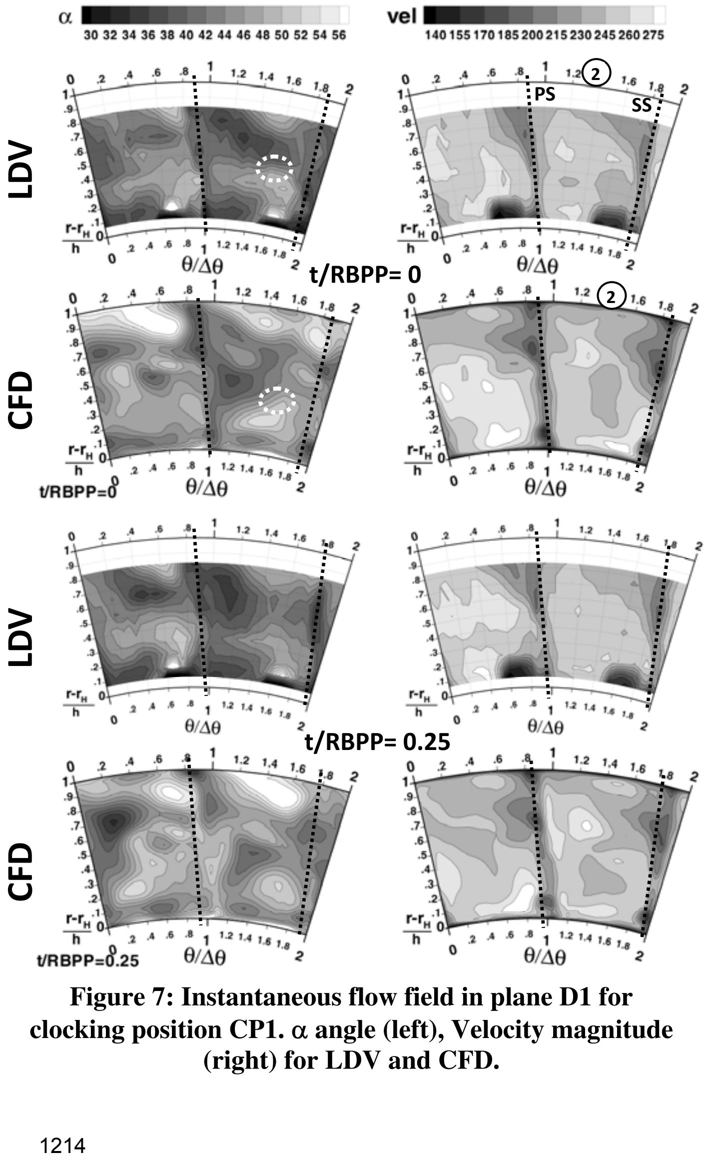

Figure 7: Instantaneous flow field in plane D1 for clocking position CP1. α angle (left), Velocity magnitude (right) for LDV and CFD.

over the whole measuring plane; the velocity contours show low fluctuations in magnitude in the free stream region as well as in the wake. On the contrary the flow angle shows fluctuations in the midspan region on the PS of the wake. These fluctuations are of minor intensity if compared with the ones observed for CP1. To provide a quantitative information on the fluctuation induced by the rotor–stator interaction, the RMS of the periodic flow angle oscillation downstream of the second vane was computed, for experiments and simulations, for the two clocking positions (Figure 9, in which the second vane is placed in the same circumferential position to improve the comprehension). The RMS indicates that the second stator wake is affected by large unsteadiness in both the two configurations. Nevertheless, outside from the wake the CP1 configuration is clearly more affected by the unsteadiness, especially around midspan.

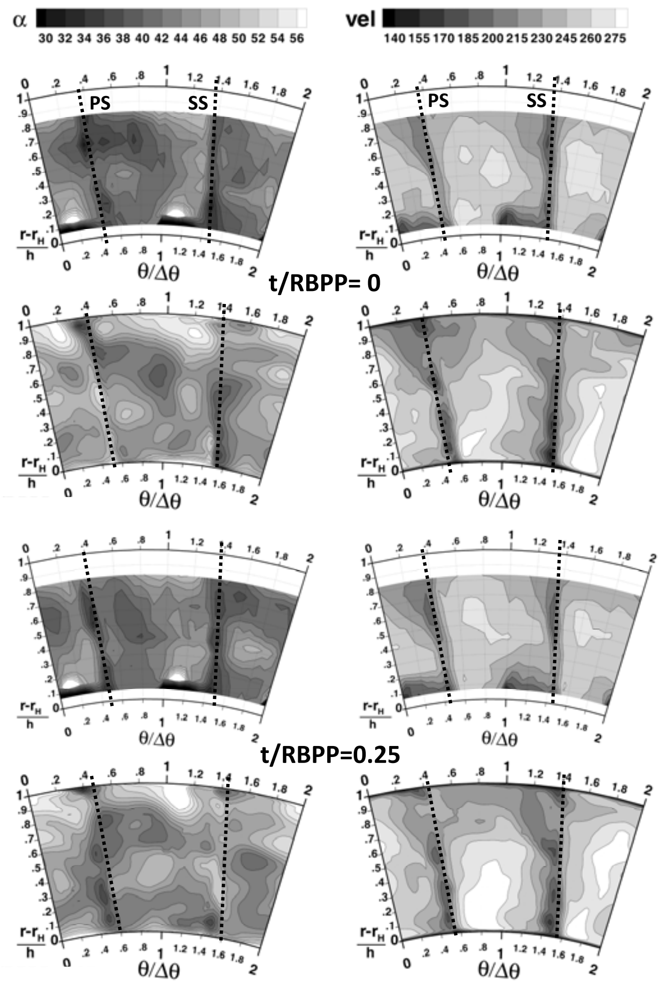

Figure 8: Instantaneous flow field in plane D1 for clocking position CP6. α angle (left), Velocity magnitude (right) for LDV and CFD.

The authors suggest that this phenomenon is linked with the spatial interaction of the incoming RHPV with the second vane; what has a periodicity in time caused by the interaction of the rotor with the 1st stator TE shock results in a periodicity in space when a second stator is located downstream of the first stage. In the previous section a strong RHPV has been shown to enter close to the PS for CP1, while it interacts with the LE of the second stator close to the PS for CP6. When the vortex impinges on the PS it probably undergoes to instability phenomena, resulting evanescent at the blade exit; on the opposite the vortex filament entering close to the SS is stretched and re-oriented, generating a second vortex whose intensity is linked to the incoming vortex. These observations are consistent with the flow visualizations reported in Sharma et al. (1992) where the effect of injecting streamwise vortices in different pitchwise position, with respect to the airfoil LE, was studied in details. More recent studies (van de Wall et al. 1996) suggested that the onset of large instability, observed also in our case when the vortex impinges the PS of the LE (CP6), was actually caused by the breakdown of vortex approaching the stagnation region. This instability process it is not activated when, instead, the vortex impinges the SS (CP1); in this case a more coherent vortex transport occurs inside the

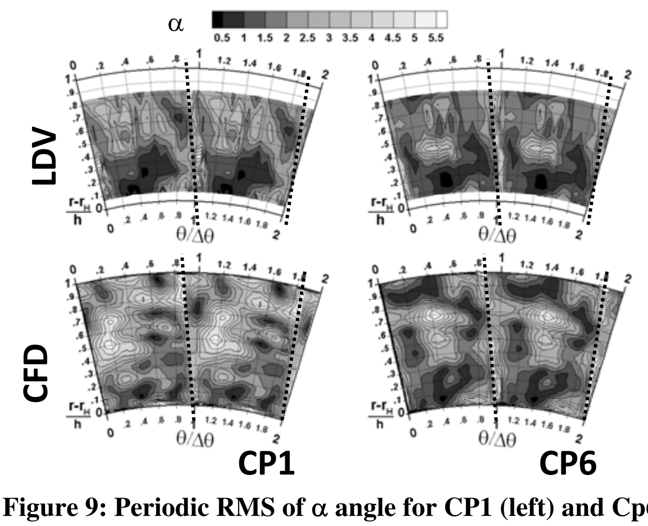

Figure 9: Periodic RMS of α angle for CP1 (left) and Cp6 (right) for experiments (top) and simulations (bottom)

channel resulting in wide and highly dissipative vortical structure downstream of the second vane.

SECOND STATOR PERFORMANCE

On the basis of the phenomenological discussion presented in the previous sections, some general considerations can be drawn by analyzing the overall averaged loss coefficient of the second stator blade row and the flow angle at plane D1. The standard definition of the total pressure loss coefficient is used , with reference to an overall averaged value of Pt in plane C2.

The configuration CP6 evidences a second stator total pressure loss (Y) reduction of about 0.6% with respect to CP1 considering FHP measurements and of about 1.2% using CFD data; smoother flow angle profiles downstream of the second stator are also observed (Figure 6), resulting in lower mixing losses downstream of the measuring section. CP1 results as the worst configuration among the 4 tested.

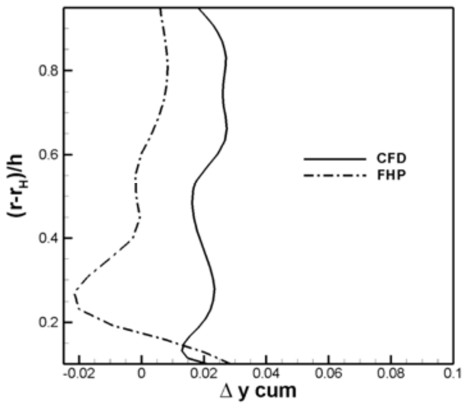

Figure 10: Cp1-Cp6 difference of cumulative loss for experiments and simulations.

The difference in the total pressure loss coefficient, although very small, is consistent with the uncertainty interval (Schennach et al., 2008a).

In Figure 10, the effect of clocking on the overall loss generation in the experiments and the simulations is reported. In particular, the cumulative loss is computed along the blade span, and the difference between Cp1 and Cp6 is plotted. The radial trends indicate that the higher effect of clocking detected in the CFD is mainly produced in the hub region, in particular between 15% span and 40% span. Above midspan, instead, the trends does not indicate significant variations, suggesting that the clocking does not affect the performance in this region both in the experiments and in the simulations. This higher effect of clocking, concentrated in the hub region and detected in computations performed without modelling the hub leakage, suggests that the presence of the hub clearance, in the experimental setup, actually reduces the possible benefits of clocking.

CONCLUSIONS

In this paper the three-dimensional unsteady character of the rotor/2nd vane interaction in a one and a half stage transonic turbine have been investigated, by means of both experimental and numerical tools. In the first part of the paper the flow field in the first stage has been considered, and the effects of the blade row interaction on the rotor-exit unsteadiness have been characterized. In particular the stator trailing edge shock has been found to be the main source of periodic unsteadiness of the rotor exit shock and of the rotor hub secondary flows.

Then the interaction of the highly unsteady rotor hub passage vortex with the second stage has been investigated using experimental data and CFD. Results evidenced that the vortical structures interact with the second stator in different ways depending on the indexing; in particular for CP1 the rorto hub passage vortex reaches its maximum magnitude when it is close to the suction side of the airfoil, while for CP6 this feature occurs when it enters close to the airfoil pressure side.

The link between the incoming three-dimensional flow features and the second vane flow field has been discussed, focusing on the effects of airfoil indexing mainly which are located at the hub. In this region where the strong hub leakage largely affect the experimental data, the flow field predicted by the fully 3D unsteady CFD simulation has provided a valid tool for the evaluation of the three-dimensional overall effects of clocking.

As a general conclusion, the strong incoming vortex is observed to produce more relevant effects when entering close to the suction side of the second vane (CP1). The onset of vortex instability probably inhibits the vortex-second stator interaction when the RHPV enters close to the PS.

These mechanisms also produce detrimental effects on the second stator performance; an increase of total pressure loss of about 0.6% from experimental data and 1.2% from CFD has been found for CP1 with respect to CP6. Moreover, on the basis of the analysis of the flow upstream of the second stator, the midspan-hub region was found to be the most potential for performance improvement thanks to airfoil indexing, due to the stronger effect of the first stator shock.

ACKNOWLEDGEMENTS

This work was made possible by the Austrian Science Fund (FWF) within the grant P16521-N07 "Experimental Investigation of the Stator-Rotor-Stator Interaction in a Transonic Turbine". The support of Dr. H. P. Pirker in the operation of the compressor station is also gratefully acknowledged.

REFERENCES

Behr, T., Kalfas, A. I., Abhari, R. S., 2007, "Stator-clocking effects on the unsteady interaction of secondary flows in a 1.5-stage unshrouded turbine", I. Mech. E. Journal of Power and Energy, Vol. 221, pp. 779-792.

Dénos R, Arts T., Paniagua G., Michelassi V., Martelli F.,2001, "Investigation on the Unsteady Rotor Aerodynamics in a Transonic Turbine Stage", ASME J. Turbomachinery, Vol. 123(1), pp 81-90.

Erhard, J., and Gehrer, A., 2000, "Design and Construction of a Transonic Test Turbine Facility," ASME Paper No. 2000-GT-480.

Gadea, J., Dénos, R., Paniagua, G., Billiard, N., and Sieverding, C. H., 2004, "Effect of Clocking on the Second Stator Pressure Field of a One and a Half Stage Transonic Turbine," ASME Paper No. 2004-GT-53463.

Haldeman, C. W., Dunn, M. G., Barter, J. W., Green, B. R., and Bergholz, R., F., 2005, "Experimental Investigation of Vane Clocking in a One and One-Half Stage High Pressure Turbine," ASME J. of Turbomachinery, Vol 127(3), pp.512-521.

Huber, F. W., Johnson, P. D., Sharma, O. P., Staubach, J. B., and Gaddis, S. W., 1996, "Performance Improvement Through Indexing of Turbine Airfoils: Part 1-Experimental Investigation," ASME J. of Turbomachinery, 118(4), pp. 630-635.

Miller, R. J., Moss, R. W., Ainsworth, R. W., and Horwood, C. K., 2003a, "Time-Resolved Vane-Rotor Interaction in a High-Pressure Turbine Stage," ASME J. Turbomachinery, 125(1), pp. 1-13.

Neumayer, F., Kulhanek, G., Pirker, H. P., Jericha, H., Seyr, A., and Sanz, W., 2001, "Operational Behavior of a Complex Transonic Test Turbine Facility," ASME Paper No. 2001-GT-489.

Paradiso B., Schennach O., Persico G., Gaetani P. , Pecnik R., Woisetschläger J., 2008, "Blade row interaction in a one and a half stage transonic turbine focusing on three dimensional effects: part I – STATOR – ROTOR INTERACTION", ASME Paper No. GT2008-50291.

Pecnik, R., Pieringer, P., Sanz, W., 2004, "Numerical Investigation of the Secondary flow of a Transonic Turbine Stage Using Various Turbulence Closures", ASME Paper No. GT2005-68754.

Pecnik, R., Sanz, W., 2006, "Application of the Turbulent Potential Model to Heat Transfer Predictions on a Turbine Guide Vane", ASME Paper No. GT2006-90365.

Perdichizzi A., 1990, "Mach Number Effects on Secondary Flow Development of a Turbine Cascade", ASME J. of Turbomachinery, Vol. 112, pp. 643-651.

Persico G., Gaetani P., Guardone A., 2005, "Design and analysis of new concept fast-response pressure probes", Meas. Sci. Technol. , Vol. 16, pp. 1741-1750.

Schennach, O., Woisetschläger, J., Marn, A., Göttlich, E., 2007, "Laser–doppler–velocimetry measurements in a one and a half stage transonic test turbine with different angular stator–stator positions", Exp. Fluids, Vol. 43, pp.385-393.

Schennach O., Pecnik R., Paradiso B., Göttlich E., Marn A., Woisetschläger J., 2008a, "The Effect of vane clocking on the unsteady flow field in a one and half stage transonic turbine", ASME J. of Turbomachinery, Vol. 130 (3).

Schennach O., Paradiso B., Persico G., Gaetani P. , Woisetschläger J., 2008b, "Blade row interaction in a one and a half stage transonic turbine focusing on three dimensional effects: part II – CLOCKING EFFECTS", ASME Paper No. GT2008-50065, accepted for the ASME J. of Turbomachinery.

Sharma O.P., Pickett G.F., Ni R.H., 1992, "Assessment of Unsteady Flows in Turbines", ASME J. of Turbomachinery, Vol. 114(2), pp. 79-90.

Van de Wall A. G., Kadambi J. R., Boyle R. J., Adamczyk J. J., 1996, "The transport of vortices through a turbine cascade", ASME J. of Turbomachinery, Vol.118(4), pp. 654–662.

Weiss A. P. ; Fottner L., 1995 , "The influence of load distribution on secondary flow in straight turbine cascades", ASME J. of Turbomachinery., Vol. 117(1), pp. 133-141.